Received: 28 December 2023 | Revised: 10 April 2024 | Accepted: 13 April 2024

DOI: 10.1002/app.55627

RESEARCH ARTICLE

Applied Polymer Science WILEY

Identification of percolation threshold of spray-dried cellulose nanocrystals in homopolymer polypropylene composites

Xueqi Wang[1] | Pixiang Wang[2] | Shaoyang Liu[2] | Ke Zhan[1] | Brian Via[1] | Tom Gallagher[1] | Mathew Smidt[3] | Douglas J. Gardner[4,5] | Thomas Elder[3] | Yucheng Peng[1]

[1]College of Forestry, Wildlife, and Environment, Auburn University, Auburn, Alabama, USA

[2]Department of Chemistry and Physics, Troy University, Troy, Alabama, USA

[3]USDA-Forest Service, Southern Research Station, Auburn, Alabama, USA

[4]School of Forest Resource, University of Maine, Orono, Maine, USA

[5]Advanced Structures and Composites Center, University of Maine, Orono, Maine, USA

Correspondence
Yucheng Peng, College of Forestry, Wildlife, and Environment, Auburn University 602 Duncan Drive, Auburn, AL 36849, USA.
Email: yzp0027@auburn.edu

Funding information
Southern Research Station, Grant/Award Number: G00013505; Alabama Agricultural Experiment Station, Grant/Award Number: ALA031-1-19091; National Institute of Food and Agriculture, Grant/Award Number: ALAZ 00079

Abstract

Understanding the percolation threshold is essential for determining the performance of particle-reinforced polymer composites. Spray-dried cellulose nanocrystals (SDCNC) of micrometer size reinforced homopolymer polypropylene (HPP) composites at 20, 30, 40, and 50 wt.% were prepared to investigate the percolation threshold of SDCNC particles in HPP. The effect of a compatibilizer (maleic anhydride polypropylene (MAPP)) at 3, 5, and 7 wt.%, on the SDCNC percolation networks and composites performance were also studied. The results indicated that SDCNC particle percolation networks in HPP were established between 30 and40 wt.%. For composites without MAPP, the impact strength significantly increased by up to 23% below the percolation threshold and declined beyond it. The peak crystallization temperature of HPP was steadily increased until 30 wt.% SDCNC particles were added due to the SDCNC saturated nucleation function at the threshold. Introducing MAPP significantly improved tensile strength (58%), tensile strain (61%), flexural strength (45%), and impact strength (91%) compared with the corresponding composites without MAPP, attributed to the enhanced interfacial adhesion between the SDCNC particles and HPP. Water absorption results indicated that adding MAPP changed the SDCNC particle distribution networks within the matrix above the percolation threshold but did not change it below the threshold.

KEYWORDS

cellulose and other wood products, composites, mechanical properties, polyolefins, thermoplastics

1 | INTRODUCTION

The wide range of applications of polypropylene (PP), including packaging, automobile, construction, toys, and furniture, makes it one of the most utilized commodity thermoplastics, due to its excellent barrier properties, moisture and chemical resistance, lightweight, moldability, and durability.[1–3] However, it has some limitations that should be considered in various applications, such as the low impact strength of the homopolymer PP (HPP),

making it prone to brittle failure. Synthetic or natural reinforcements or fillers are generally used to enhance mechanical performance, including toughness, to overcome uncompetitive mechanical properties. Synthetic fillers such as glass or carbon fibers, talc, calcium carbonate, nanoclay, and carbon nanotubes have been widely studied for reinforcing PP composites.[4–9] The growing concerns about environmental issues has led to increased interest in incorporating natural fillers, such as wood flour, jute, rice husks, and cellulose fibers, in PP composites.[10–13] Cellulose fibers, possessing numerous advantages such as lightweight, renewable, and biodegradable, are a competitive filler that can enhance the composites performance.[14–16] Spray-dried cellulose nanocrystal (SDCNC) particles, a dry form of cellulose-based particles, have shown potential in fabricating PP composites via a cost-effective and solvent-free melt compounding process.[17–20] Research on developing the SDCNC PP matrix composites with high performance using a melt compounding process attracts interest from academia and industry.

Generally, designing particle-reinforced polymer matrix composites is concerned with the maximum efficiency for polymer property improvement and the maximum loading level of particles in the matrix.[21] Establishing percolation networks of particles within the polymer matrix is a primary cut-off criterion for the composite performance.[22–25] Percolation describes the dispersion of particles in a random system to form larger connected clusters spanning across the entire system at a certain critical volume fraction, referred to as the percolation threshold.[26]

Numerous literatures showed that the percolation threshold of nanosized rod-like cellulose nanocrystal (CNC) varies among different polymer matrices.[27–33] Santamaria-Echart et al.[30] evaluated the CNC percolation threshold in a waterborne polyurethane matrix by measuring the tensile and thermomechanical properties of the resulting nanocomposites. In this study, enhancements in tensile stress at yield (36%), tensile modulus (16%), and thermomechanical stability were observed at the CNC percolation threshold (3 wt.% CNC). Sheets of styrene butadiene rubber (SBR) reinforced with varying levels of CNC from 0.5 to 8 wt.% (based on rubber weight) were fabricated by a solution casting process.[28] The tear strength and maximum work required to tear the sheets increased at CNC loading level above 4 wt.% in the SBR latex, at which point the percolation of CNC occurred. Two CNC percolation thresholds at around 0.8 and 1.5 wt.% in poly(butylene succinate) (PBS) matrix were revealed and the mechanical and hydrolytic properties of CNC-PBS nanocomposites showed significant changes at the threshold.[29] As discussed above, CNC particles in solution or latex can building a continuous rigid network through hydrogen bonds at the percolation threshold, thereby dramatically improving the performance of polymer composites.[33]

However, for SDCNC particles, the particle size (microscale), morphologies, and surface energy differs dramatically from CNC on a nanoscale, which are the factors influencing the threshold.[19,33–37] In addition, hydrogen-bonded SDCNC particle networks cannot be built in the melt compounding process as the networks are established during the solution casting process by the solvent drying process.[38] Therefore, the effect of percolation threshold on composite performance is entirely different for SDCNC particles in a thermoplastic matrix manufactured using a melt compounding process. In more detail, the contact point between SDCNC particles could function as a discontinuity surface rather than forming strong hydrogen bonds, facilitating composite failure under external stress. Surpassing the percolation threshold could also potentially lead to SDCNC particle agglomeration, inducing stress concentration points and weakening the effective stress transfer from SDCNC to the polymer matrix.[39] Hence, research on evaluating the percolation threshold of SDCNC particles in polymer matrix is beneficial for developing high-performance SDCNC PP composites.

The other challenge associated with developing high-performance PP composites using SDCNC particles is the inherent incompatibility between the hydrophilic SDCNC and the hydrophobic PP, which leads to poor interfacial adhesion between the components, a key factor influencing the tensile strength of composites.[21] Maleic anhydride-grafted polypropylene (MAPP) is commonly used to effectively increase the interfacial adhesion between cellulosic fillers and PP matrix due to the low cost, simple process, and absence of extra solvents compared with other chemical surface treatments.[2,40–42] It is worth noting that MAPP may also change the SDCNC particles interaction, which would affect the percolation networks.[33] Therefore, the effect of adding MAPP on the percolation networks of SDCNC particles in polymer matrix deserves to be evaluated.

Understanding the percolation threshold of SDCNC particles in polymer matrix can help to determine the maximum loading level of SDCNC particles in the composite, facilitating to achieve the highest efficiency in enhancing the composites performance. This research aimed to search the SDCNC particle percolation threshold within HPP composites to optimize the composite performance reinforced by SDCNC particles. The effect of adding the compatibilizer MAPP on the SDCNC percolation threshold in the HPP matrix was also investigated. A water absorption experiment was performed to understand the diffusion of water molecules into the SDCNC

particle reinforced HPP composites. The hypothesis was that the percolation network of SDCNC particles in the HPP significantly impacts the water absorption due to the particle hydrophilicity. Measurement of the water absorption of SDCNC reinforced HPP composites can be used to characterize the SDCNC particle percolation threshold in the composites. The effect of the percolation threshold, which was evaluated from water absorption measurement, on the mechanical and thermal properties of the composites was also studied. The resulting composites with enhanced stiffness and strength can expand the applications of HPP in many fields, including packaging, automobile, construction, and toys and so on.

2 | MATERIALS AND METHODS

2.1 | Materials

The HPP pellets (ExxonMobil™ PP1264E1) with a density of 0.9 g cm^{-3} and a melt flow index of 20 g 10 min^{-1} (230°C 2.16 Kg^{-1}) were received from ExxonMobil Chemical Company (Houston, TX). The SDCNC powder derived from sulfuric acid hydrolysis was obtained from CelluForce (Montreal, Canada). The characterization of the SDCNC particles was detailed in the previous publication.[19] MAPP (Polybond 3200) pellets were supplied by ChemPoint Inc. (Bellevue, WA, USA), with a melt flow index of 115 g 10 min^{-1} (190°C 2.16 Kg^{-1}), a density of 0.91 g cm^{-3}, and a melting point of 157°C and a maleic anhydride content in the range of 0.8%–1.2%.

2.2 | Composite manufacturing

The composite formulations are shown in Table 1. A masterbatch method was used to prepare SDCNC-reinforced HPP composites. An internal mixer (C.W. Brabender CWB-2128, Hackensack, NJ, USA) was used to manufacture all composites at 200°C with the two mixing blades rotating counterclockwise at 60 rpm. The SDCNC powder and MAPP pellets were oven-dried at 105°C overnight to remove any potential moisture before melt compounding. The HPP pellets were first melted in the mixer until a constant torque was achieved (5 min). Then, the SDCNC particles were added into the mixing chamber for further compounding for an additional 5 min to reach a constant torque value. The masterbatch with 50 wt.% SDCNC was prepared first. The masterbatch for the composite with MAPP was prepared by mixing HPP and the designated amount of MAPP first, followed by adding the SDCNC particles. After thermal compounding, the cooled mixture was ground into a pellet form using a granulator (Shini Plastic Technologies Inc., Willoughby, OH, USA). For the fabrication of the final composites as shown in Table 1, the oven-dried masterbatch pellets and the designed amount of fresh HPP pellets were dry-mixed and then compounded for 5 min in the mixer to reach a constant torque value. The final mixed composites were then ground into pellets and oven-dried at 105°C overnight prior to being processed into standard-shaped samples for mechanical properties evaluation according to ASTM D638 (Type IV), ASTM D790-A, and ASTM D256, respectively.

An injection molding machine (Proto-Ject 150HP, Manning Innovations Inc., Halls, TN, USA) at 200°C and a pressure of 44 MPa was used for all composite specimen manufacturing. After molding, the samples were placed in Ziploc bags and stored in desiccators at room temperature for at least 48 h to prevent moisture absorption before testing. Pure HPP pellets prepared with the same melt compounding and injection molding process were used as a control sample. The sample names are listed in Table 1, where SDCNC-reinforced

TABLE 1 The formulations of SDCNC/HPP and SDCNC/MAPP/HPP composites.

Sample name	HPP (wt.%)	SDCNC (wt.%)	MAPP (wt.%)
HPP	100	0	0
20CNC	80	20	0
30CNC	70	30	0
40CNC	60	40	0
50CNC	50	50	0
30CNC3MAPP	67	30	3
30CNC5MAPP	65	30	5
30CNC7MAPP	63	30	7
40CNC3MAPP	57	40	3
40CNC5MAPP	55	40	5
40CNC7MAPP	53	40	7

HPP composites without MAPP (SDCNC/HPP) pellets were denoted as aCNC (a is the SDCNC weight percentage in the composite based on the total weight of composite), and SDCNC-reinforced HPP composites with MAPP pellets (SDCNC/MAPP/HPP) was denoted as bCNCcMAPP (b and c are the SDCNC and MAPP weight percentages based on the total weight of the composite).

2.3 | Mechanical properties testing

The evaluation of mechanical properties of all composites, including tensile, flexural, and impact properties, was performed according to ASTM D638, D790-A, and D256, respectively. A Mark-10 ESM750s motorized test machine (Copiague, NY, USA) with a 2500-N load cell was used to perform tensile tests at a cross-head speed of 5 mm min^{-1}. The strain of composites was measured by an Epsilon extensometer SN E109112 (Jackson, WY, USA). At least five specimens from each formulation were tested for tensile properties. Flexural tests were performed using a Mark-10 ESM750s motorized test machine (Copiague, NY, USA) equipped with a 500-N load cell at a cross-head speed of 1.34 mm min^{-1}. Five specimens from each formulation were tested for flexural properties. The notched Izod impact tests were carried out with a Zwick/Roll HIT 25P (Germany) impact tester equipped with a 1 J pendulum for SDCNC/MAPP/HPP composites. A V-shape notch with a depth of 2.54 mm and a notch angle of 45° was created using a manual Instron CEAST notcher (Norwood, MA, USA) prior to conducting the impact test for all specimens. Ten specimens from each formulation were tested for impact strength (kg m^{-2}). All tests were conducted at room temperature of 23 ± 2°C with 50% ± 5% RH.

2.4 | Water absorption testing

Water absorption tests were conducted according to ASTM D570. Five impact fractured specimens from each formulation were used for the water absorption experiment. All specimens were conditioned by oven drying at 105°C to a constant weight. Afterward, the specimens were weighed to the nearest 0.0001 g before immersing them in deionized water at a room temperature of 23 ± 2°C for a long duration (150 days). At specific time intervals (every day in the first week, one or two week intervals after that), the specimens were removed from the water and dried with Kimtech kimwipes, followed by weight and thickness measurement, and then replaced into the water. The percentages of water gain and thickness swell were calculated and recorded. The diffusion coefficients (D) of water molecules for all composites were calculated according to the following model[43,44]:

$$D = \pi \left(\frac{h}{4M_\infty}\right)^2 \left(\frac{M_2 - M_1}{\sqrt{t_2} - \sqrt{t_1}}\right)^2, \quad (1)$$

where M_∞ is the equilibrium water gain (assumed to be the maximum water gain at the end of the experiment (150 days)), h is the sample thickness, M_2–M_1 is the water gain variation at the initial linear region, $\sqrt{t_2} - \sqrt{t_1}$ is the square root of the time variation at the initial linear region.

2.5 | Morphological properties

A Zeiss Evo 50VP scanning electron microscope (SEM) (Oberkochen, Germany) was used to examine the Izod impact-tested cross-section surfaces of all the composites to evaluate the morphological properties. An accelerating voltage of 20 kV was used for the SEM work. The specimen surfaces were sputter-coated with gold for 60 s by a Q150R ES sputter coater (Hatfield, PA, USA) before SEM observation.

2.6 | Thermal characterization

Differential scanning calorimetry (DSC) analysis was performed using a TA instrument DSC-250 (DE, USA) under a nitrogen atmosphere with the following conditions: (1) heating about 10–15 mg sealed sample from 40 to 200°C, (2) holding at 200°C for 2 min to eliminate the previous thermal history, (3) cooling to 40°C, (4) isothermal at 40°C for 2 min, (5) reheating to 200°C. Both heating and cooling rates were 10°C min^{-1}. The cooling and second heating thermograms were analyzed using the TRIOS (TA Instruments, DE, USA) software. At least duplicates were tested for each sample. The crystallinity X_c (%) was calculated using the following equation[42]:

$$X_c\,(\%) = \frac{\Delta H_m}{\Delta H_m^0\, w_{HPP}} \times 100\%, \quad (2)$$

where ΔH_m is the melting enthalpy obtained from the second heating cycle; ΔH_m^0 is the melting enthalpy of HPP with 100% crystallinity extracted from the literature (205 J mol^{-1})[45]; and w_{HPP} is the weight ratio of HPP in the composite.

TABLE 2 The mechanical properties of SDCNC/HPP composites.

Sample	Tensile properties			Flexural properties		
	MOE (GPa)	Strength (MPa)	Strain (%)	MOE (GPa)	Strength (MPa)	Impact strength (kJ m^{-2})
HPP	1.34 ± 0.03[a] E[b]	30.2 ± 0.2 A	10.3 ± 0.6 A	1.32 ± 0.02 E	40.7 ± 0.5 B	1.59 ± 0.12 B
20CNC	2.05 ± 0.09 D	26.1 ± 0.6 B	5.2 ± 0.5 B	1.72 ± 0.04 D	42.9 ± 0.9 A	1.85 ± 0.15 A
30CNC	2.38 ± 0.10 C	22.6 ± 0.3 C	3.9 ± 0.3 C	2.04 ± 0.02 C	42.4 ± 0.3 A	1.95 ± 0.21 A
40CNC	2.68 ± 0.12 B	20.3 ± 0.4 D	2.8 ± 0.1 D	2.46 ± 0.02 B	39.5 ± 0.5 C	1.48 ± 0.25 B
50CNC	2.99 ± 0.23 A	17.7 ± 0.5 E	2.2 ± 0.3 E	2.87 ± 0.08 A	35.0 ± 0.3 D	1.39 ± 0.10 B

[a]Mean value and standard deviation.
[b]For each column, different letters represent the significant difference ($p < 0.05$).
Abbreviation: MOE, modulus of elasticity.

2.7 | Statistical analysis

One-way ANOVA (analysis of variance) with a 0.05 significance level, followed by Tukey's post-hoc tests, was applied to analyze the mechanical properties of SDCNC/HPP composites and the water absorption properties of all composites separately. The effect of different loadings of SDCNC and MAPP on each mechanical property was analyzed using two-way ANOVA with Tukey's post-hoc tests at a 0.05 significance level. The two-factor model was:

$$Y_{ijk} = \mu + \alpha_i + \beta_j + \gamma_{ij} + \varepsilon_{ijk} \sim N(0, \sigma), \quad (3)$$

where $i = 1, 2$; j = 1, 2, 3, 4; $k = 1, 2, 3, 4, 5, 6, 7$ (tensile properties) or 1, 2, 3, 4, 5 (flexural properties) or 1, 2, 3, 4, 5, 6, 7, 8, 9, 10 (impact properties); Y_{ijk} is the mean value of each mechanical property tested; μ is the population mean value of each mechanical property; α_i and β_j are the effects of SDCNC and MAPP contents on the mechanical properties; γ_{ij} is the interaction effect between SDCNC and MAPP on the mechanical properties; and ε_{ijk} is the error associated with a normal distribution (N) and standard deviation (σ).

3 | RESULTS AND DISCUSSIONS

3.1 | Mechanical properties of SDCNC/HPP composites

The effect of various loadings (20, 30, 40, and 50 wt.%) of SDCNC particles on the mechanical properties of the composites was evaluated (Table 2). The representative tensile stress–strain curves of neat HPP and SDCNC/HPP composites are shown in Figure 1. The incorporation of high-stiffness SDCNC (around 100–130 GPa) resulted in all SDCNC/HPP composites having greater tensile modulus of elasticity (MOE) values than neat HPP (1.34 ± 0.03 GPa).[46] The tensile moduli increased as the SDCNC content increased, reaching up to 2.99 ± 0.23 GPa for 50CNC, which was 123% higher than that of neat HPP. In contrast, the tensile strength and tensile strain at the yield point decreased monotonically with increasing SDCNC content compared with neat HPP (Table 2). The decrease was ascribed to the incompatibility between hydrophilic SDCNC particles and hydrophobic HPP matrix, generating separated interfacial space (Figures 2c–f) and an ineffective stress transfer. The addition of rigid SDCNC particles could restrict the mobility of polymer chains and reduce the ductility of the composites.[47,48]

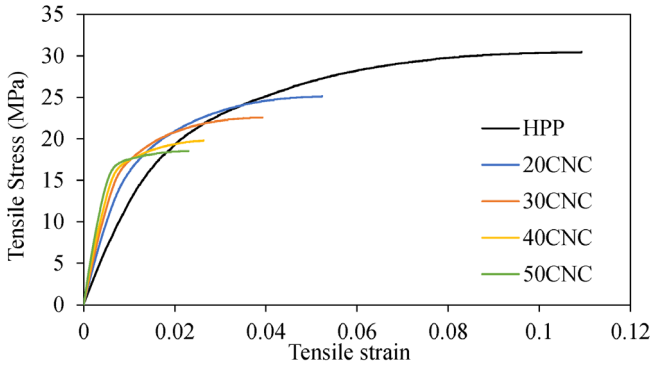

FIGURE 1 The representative tensile stress–strain curves of SDCNC/HPP composites. [Color figure can be viewed at wileyonlinelibrary.com]

The representative flexural stress–strain curves of neat HPP and SDCNC/HPP composites are shown in Figure 3. The flexural MOE of SDCNC/HPP composite steadily increased with increasing SDCNC content, reaching up to 2.87 ± 0.08 GPa for 50CNC, approximately 117% higher than that of neat HPP (Table 2). This trend aligns well with the change in tensile MOE. Flexural strength, reported as the stress at yield point for 30CNC, 40CNC, and 50CNC and the stress at 5% strain

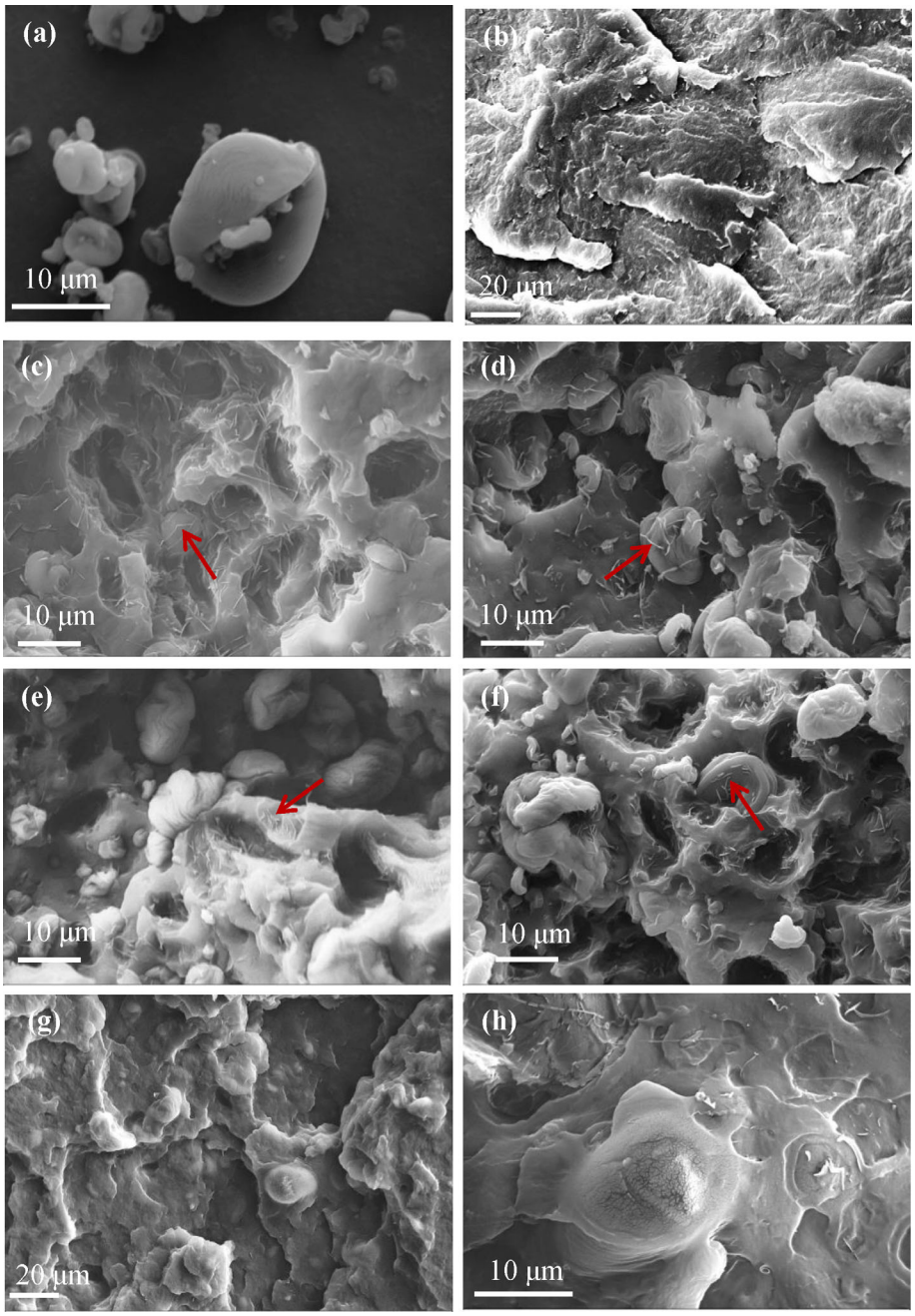

FIGURE 2 The morphology of SDCNC particles (a), the fracture surface morphologies of composites: HPP (b), 20CNC (c), 30CNC (d), 40CNC (e), 50CNC (f), and 30CNC5MAPP (g and h). [Color figure can be viewed at wileyonlinelibrary.com]

for HPP and 20CNC (no yield or break before 5% strain according to the ASTM D790-A), demonstrated a complex relationship. A significant increase in flexural strength occurred for 20CNC and 30CNC, followed by a significant decrease for 40CNC and 50CNC. Unlike the tensile test, the complex deformation experienced by the composites during the flexural test, combining the compression on the top surface and the tension on the bottom surface of composites. For 20CNC and 30CNC, the increase in the compression strength on the top surface during flexural test coupled with the increase in the stress required for the bottom surface to reach the 5% strain or yield point, contributed to the increase in the flexural strength. But the higher filler content formed large aggregates and introduced extra stress concentration points in the composite, impeding the stress transfer. Consequently, the flexural strength decreased at higher filler loading levels.

The impact strength of SDCNC/HPP composites increased initially with 20 and 30 wt.% of SDCNC, peaking at 1.95 ± 0.21 kJ m^{-2} for 30CNC (20% higher than that of neat HPP), then decreased to 1.48 ± 0.25 and 1.39 ± 0.10 kJ m^{-2} for 40CNC and 50CNC, showing no statistically significant differences from the neat HPP based on the statistical analysis (Table 2 and Figure 4). The physical adhesion based on the mechanical interlocking

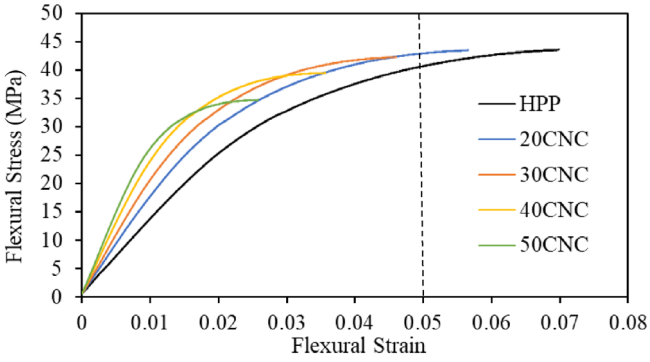

FIGURE 3 The representative flexural stress–strain curves of SDCNC/HPP composites. [Color figure can be viewed at wileyonlinelibrary.com]

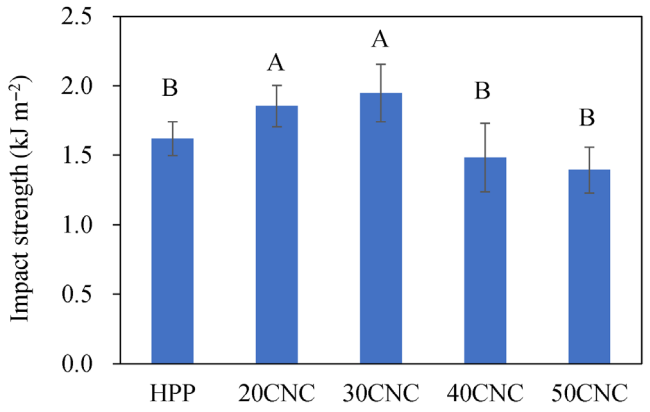

FIGURE 4 The impact strength of all SDCNC/HPP composites. [Color figure can be viewed at wileyonlinelibrary.com]

between the SDCNC particles and the HPP matrix, caused by the irregular shapes of SDCNC, was the reason for the increased impact strength.[19] This mechanical interlocking failure mode of the polymer strands with stretched filaments can be seen in the SEM micrographs shown in Figure 2c–f (red arrows). The longer polymer strands stretched during fracture shown in 20CNC and 30CNC composites indicated that higher energies were required to create the fracture surface (Figure 2c–f). However, at higher SDCNC levels (40CNC and 50CNC), large agglomerates of SDCNC particles without effective contact with the matrix formed, interrupting the integrity between SDCNC particles and the HPP matrix caused by the mechanical interlocking adhesion. Simultaneously, the fracture surface morphologies (Figure 2c–f) demonstrated the fracture paths going through spaces between SDCNC particles without involving the polymer matrix. The SDCNC particles are spray-dried, and the adhesion between the particles is weak. Hence, the impact strength decreased at higher SDCNC loading levels. The significant impact strength changes of the composites from 30CNC to 40CNC indicated a dramatic internal structure change in SDCN/HPP composites when the SDCNC loading changes from 30 to 40 wt.%.

3.2 | Water absorption properties of SDCNC/HPP composites

Water absorption testing was performed to evaluate the distribution of SDCNC particles in the HPP matrix and to explore the possible change in the internal structure of the SDCNC/HPP composites. The percentages of the water gain and thickness swell were plotted against the square root of time (Figure 5), and the initial slope of the water gain curve (25 days) was calculated to determine the water diffusion coefficient. The percentages of the water gain and thickness swell at the end of the experiment were also calculated, as shown in Table 3. For 20CNC, 30CNC, 40CNC, and all SDCNC/MAPP/HPP composites, a plateau stage representing the equilibrium water gain was not shown in Figure 5. However, the percentages of thickness swell have already approached the maximum values. Moreover, according to ASTM D570, the average increase in weight per 2 week period, calculated from 3 consecutive weighings, was less than 5 mg by the end of 150 days. Hence, the values of water gain of these composites were suggested to reach substantial saturation.

The results indicated that the neat HPP has an excellent water barrier property. The water gain and thickness increased as the SDCNC particle loading level in the composite increased because of its hydrophilic nature. Water molecules were predominately absorbed by the SDCNC particles on the composite surface, followed by diffusion into the center of the composite through three different paths: (1) connected SDCNC particles, (2) SDCNC-HPP interfaces (separated interfaces caused by the weak interfacial adhesion), and (3) HPP layer separating SDCNC and HPP. Theoretically, increasing SDCNC particle loading levels in the composite is expected to result in a proportional increment in equilibrium water gain because of the hydrophilic nature of SDCNC and the expansion of interfacial areas between SDCNC and HPP. This theory works if each individual SDCNC particle is separated from each other with HPP as the wrapping layer. This situation occurred for 20CNC and 30CNC composites, as demonstrated by the equilibrium water gains of the two composites (Table 3), that is, there is a direct proportional relationship between the SDCNC loading and the equilibrium water gain. The water gain to SDCNC loading ratios are the same for 20CNC and 30CNC (0.066 ± 0.001). However, the water gain to SDCNC loading ratios increased at higher SDCNC

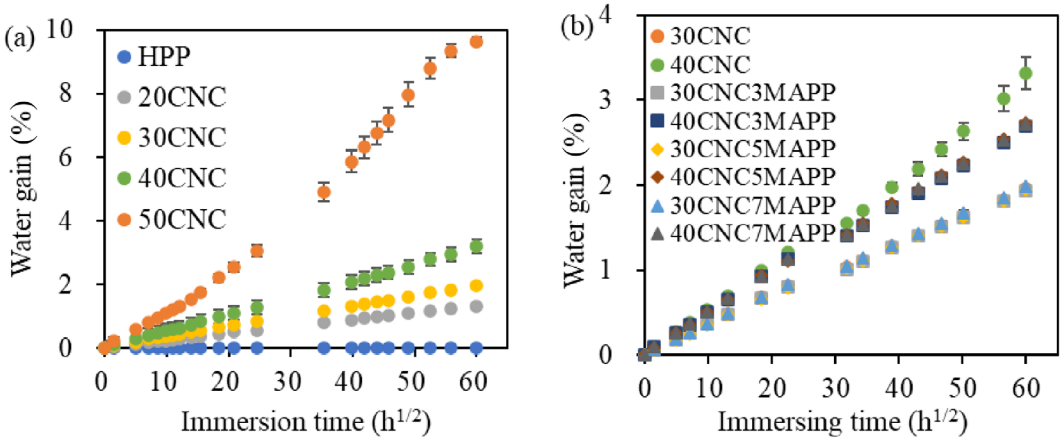

FIGURE 5 Water gain for SDCNC/HPP composites (a) and SDCNC/MAPP/HPP composites (b). [Color figure can be viewed at wileyonlinelibrary.com]

TABLE 3 Water absorption properties of SDCNC/HPP and SDCNC/MAPP/HPP composites.

Composites	Water gain (%)	Water gain/SDCNC loading ratio	Diffusion coefficient (10^{-3} mm^2 h^{-1})	Thickness swell (%)
HPP	0.02 ± 0.01[a] E[b]	-	4.81E-04 ± 2.95E-04	0.27 ± 0.05 D
20CNC	1.32 ± 0.02 D	0.066 ± 0.001	1.35 ± 0.07	0.86 ± 0.11 C
30CNC	1.97 ± 0.01 C	0.066 ± 0.001	3.60 ± 0.11	1.09 ± 0.18 C
40CNC	3.19 ± 0.01 B	0.080 ± 0.001	10.45 ± 0.62	1.88 ± 0.22 B
50CNC	9.64 ± 0.14 A	0.193 ± 0.001	87.54 ± 9.56	3.84 ± 0.17 A
30CNC3MAPP	1.94 ± 0.02	0.065 ± 0.001	3.39 ± 0.34	1.03 ± 0.02
30CNC5MAPP	1.94 ± 0.01	0.065 ± 0.001	3.63 ± 0.06	1.03 ± 0.03
30CNC7MAPP	1.99 ± 0.02	0.066 ± 0.001	3.97 ± 0.29	1.04 ± 0.05
40CNC3MAPP	2.69 ± 0.01	0.067 ± 0.001	8.44 ± 0.23	1.52 ± 0.05
40CNC5MAPP	2.74 ± 0.02	0.069 ± 0.001	8.52 ± 0.37	1.59 ± 0.05
40CNC7MAPP	2.72 ± 0.02	0.068 ± 0.001	8.57 ± 0.17	1.55 ± 0.04

[a]Mean value and standard deviation.
[b]For each parameter, different letters represent the significant difference ($p < 0.05$).

loadings, which became much greater (0.080 ± 0.002 and 0.193 ± 0.003 for 40CNC and 50CNC, respectively) (Table 3). This observation indicated that: (1) there is no considerable change in the SDCNC distribution in 20CNC and 30CNC; (2) the SDCNC distributions in 40CNC and 50CNC differ dramatically from 20CNC and 30CNC and from each other; and (3) the SDCNC percolation threshold is between 30 and 40 wt.%.

The distribution of SDCNC particles in HPP matrix was shown in Figure 6. The proposed mechanism of water absorption, based on the suggested percolation theory, is illustrated in Figure 7. The SDCNC particles were uniformly distributed in HPP, completely encapsulated by the matrix, and separated from each other in 20CNC (Figures 6a and 7a). The major water absorption pathway was the absorption and diffusion of water molecules from the specimen surface (either through SDCNC particles or HPP) and the interface between SDCNC and HPP to another phase of SDCNC or HPP inside. The diffusion rate for pure HPP was extremely low, with a diffusion coefficient of 4.81E-07 mm^2 h^{-1}, whereas 20CNC exhibited a notable 3000-fold increase. It revealed that SDCNC particles facilitated the absorption of water molecules through hydrogen bonding.[28] The diffusion coefficient of 30CNC is 160% higher than that of 20CNC. With the same ratios of water gain to SDCNC loadings, the change in the diffusion coefficient is mainly due to the increased SDCNC loading. A higher water diffusion coefficient of 30CNC may indicate local SDCNC particle agglomerates may be present, as proposed in Figure 6b and 7b. In 30CNC, HPP still encapsulated individual and locally agglomerated SDCNC particles. Consequently, the

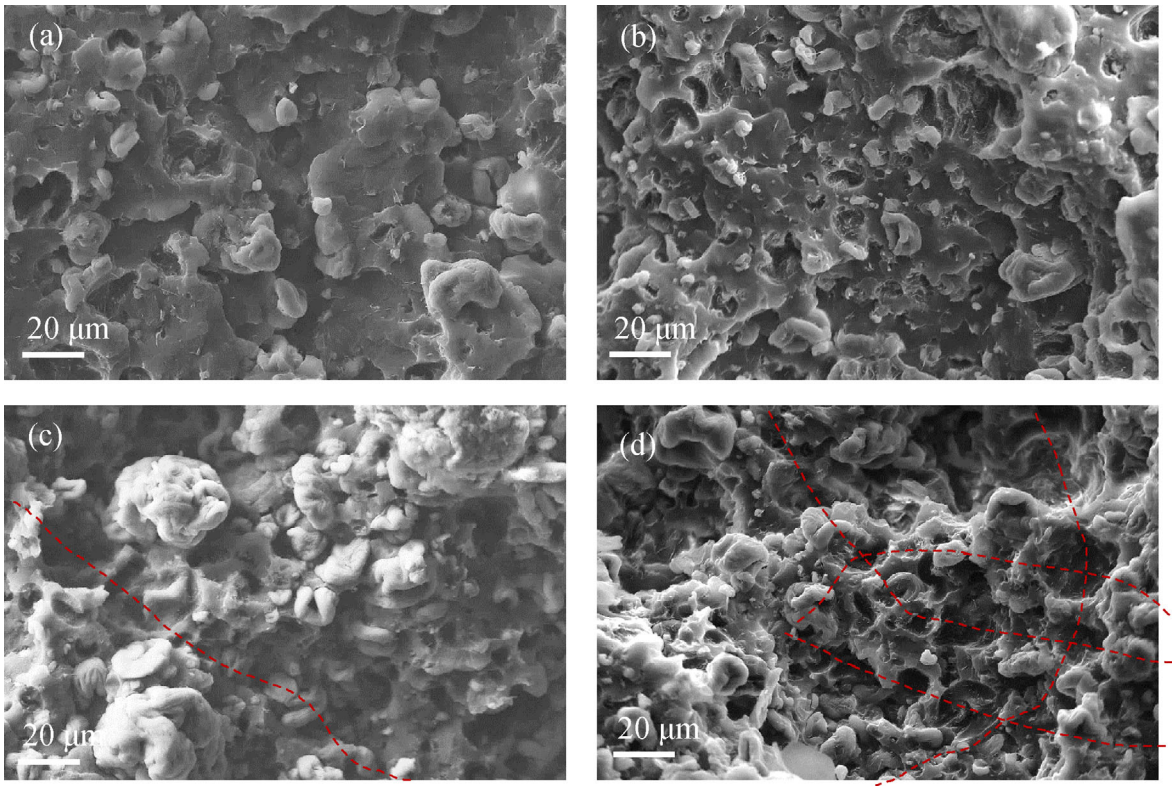

FIGURE 6 Scanning electron microscopy micrographs of SDCNC/HPP composites: 20CNC (a), 30CNC (b), 40CNC (c), and 50CNC (d). Red dash lines represent the proposed SDCNC particles percolated network. [Color figure can be viewed at wileyonlinelibrary.com]

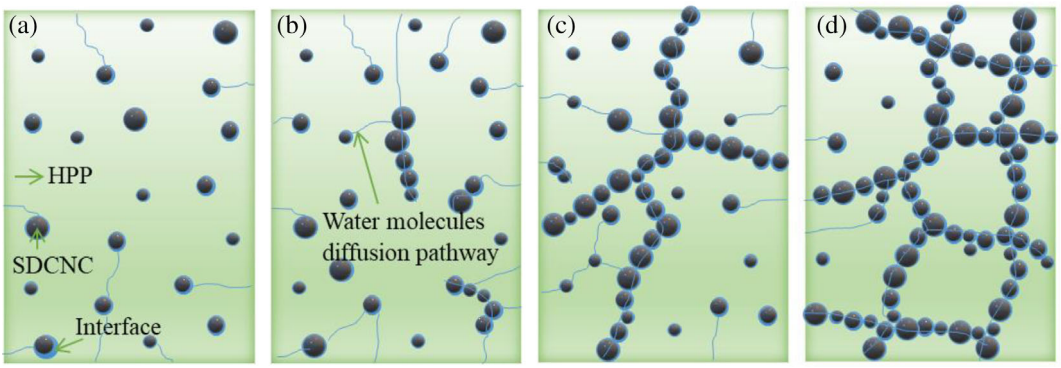

FIGURE 7 The proposed mechanism of water absorption for 20CNC (a), 30CNC (b), 40CNC (c), and 50CNC (d). HPP, homopolymer polypropylene. [Color figure can be viewed at wileyonlinelibrary.com]

matrix, the dispersed SDCNC particles, and agglomerates still predominantly govern water molecule diffusion.

As SDCNC loading further increases, the water diffusion coefficient of 40CNC increased by about seven times compared with 20CNC, which is assumed to be two times if there were no internal structure changes of SDCNC particle distribution. A proposed integrated network structure (percolation) of SDCNC particles is formed inside 40CNC. At this point, the matrix failed to encapsulate all SDCNC particles separately, and water molecules can easily be transported continuously between SDCNC particles throughout the composite structure. Simultaneously, it is proposed that only limited numbers of percolation networks were established in 40CNC (Figure 6c and 7c). Once more SDCNC percolated networks were established in 50CNC (Figure 6d and 7d), the water diffusion coefficient increased approximately 60 times compared with 20CNC. The multiple percolated SDCNC networks promote the movement of water molecules from different directions, enabling greater diffusion rates of water molecules through the composites. The high-density hydroxyl groups of SDCNC particles

TABLE 4 The thermal characterizations of all composites.

Samples	Melting process		Crystallization process		
	ΔH_m (J g^{-1})	T_m (°C)	ΔH_c (J g^{-1})	T_c (°C)	X_c (%)
HPP	84.7 ± 1.8	161.6 ± 0.9	87.0 ± 1.1	112.5 ± 0.1	41.3 ± 0.9
20CNC	69.0 ± 2.8	161.9 ± 0.3	77.4 ± 0.6	122.1 ± 0.3	43.0 ± 1.8
30CNC	62.3 ± 0.8	161.3 ± 0.4	60.5 ± 0.6	124.5 ± 0.2	43.4 ± 0.6
40CNC	54.8 ± 0.9	162.6 ± 1.1	53.0 ± 1.0	124.4 ± 0.6	44.5 ± 0.8
50CNC	46.3 ± 1.0	162.0 ± 0.4	43.1 ± 1.5	124.8 ± 1.3	45.1 ± 0.9
30CNC3MAPP	62.3 ± 1.9	161.1 ± 0.7	63.4 ± 0.6	120.1 ± 0.3	43.4 ± 1.3
30CNC5MAPP	64.4 ± 0.6	160.8 ± 0.4	65.8 ± 0.1	118.8 ± 0.2	44.9 ± 0.4
30CNC7MAPP	62.0 ± 0.5	160.9 ± 0.8	63.0 ± 0.1	118.1 ± 0.2	43.2 ± 0.4
40CNC3MAPP	54.7 ± 0.5	161.1 ± 0.3	55.2 ± 1.9	120.8 ± 0.7	44.5 ± 0.4
40CNC5MAPP	53.5 ± 1.6	160.9 ± 0.7	53.0 ± 0.7	119.4 ± 0.4	43.5 ± 1.3
40CNC7MAPP	55.0 ± 0.2	160.7 ± 0.5	53.0 ± 0.1	118.6 ± 0.2	44.7 ± 0.2

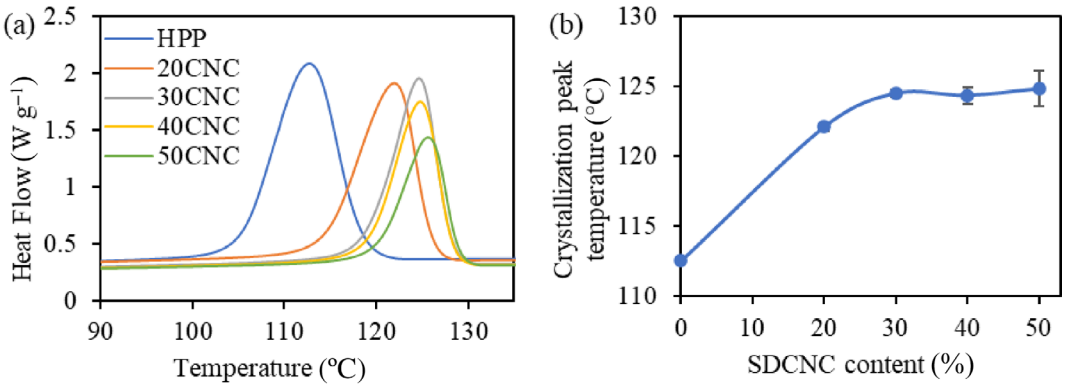

FIGURE 8 The crystallization exothermal curves of SDCNC/HPP composites (a). The relationship between crystallization peak temperature and the SDCNC loadings (b). [Color figure can be viewed at wileyonlinelibrary.com]

facilitate hydrogen bonding interactions with adjacent water molecules, allowing for the easy migration of water molecules along the SDCNC percolation networks.

3.3 | Thermal properties of SDCNC/HPP composites

The crystallization and melting behaviors of all the composites were evaluated by DSC, and the peak temperatures for crystallization and melting are summarized in Table 4. The DSC thermograms of the crystallization process are shown in Figure 8. For the SDCNC/HPP composites, the crystallization exothermal curves shifted toward higher temperatures after adding the SDCNC particles (Figure 8a). The HPP crystallization peak temperature (T_c) is 112.5 ± 0.1°C. Adding 20 wt.% SDCNC particles in the composite increased the T_c of HPP to 122.1 ± 0.3°C. This increment is caused by the nucleation function of the cellulose surface, forming a well-known transcrystalline layer around the SDCNC particles.[49,50] Adding 30 wt.% SDCNC further increased the HPP T_c to 124.5 ± 0.2°C, a minor increase compared with 20CNC composite. This observation indicated that more cellulose HPP interfacial area was created for 30CNC than for 20CNC, further increasing the nucleation function of the cellulose surface. However, further increase of the SDCNC loadings did not increase T_c of HPP in 40CNC (124.4 ± 0.6°C) and 50CNC (124.8 ± 1.3°C). The relationship between the T_c and the SDCNC loading levels is shown in Figure 8b. These results indicated that (1) the SDCNC particles acted as an effective nucleating agent in the HPP matrix,[17,51,52] inducing the formation of additional nucleation sites to facilitate the crystallization of HPP at a higher temperature; (2) the T_c of HPP changed with SDCNC loading level up to the percolation threshold due to surface nucleation function of cellulose; (3) the amounts of the SDCNC and HPP interface in 40CNC and 50CNC were similar to that in 30CNC which is slightly greater than that in 20CNC; and (4) 30 wt.%

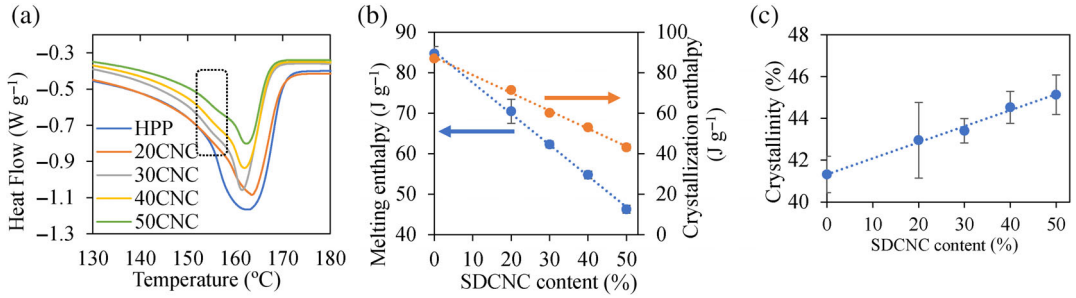

FIGURE 9 The melting endothermal curves of SDCNC/HPP composites (a), and the relationship between melting and crystallization enthalpy with SDCNC loadings (b) and the relationship between crystallinity with SDCNC loadings (c). [Color figure can be viewed at wileyonlinelibrary.com]

SDCNC particles in the HPP saturated the nucleation function of the cellulose surface for the HPP. In other words, SDCNC particles at the percolation threshold in the HPP matrix provided a maximum nucleation function, and adding more SDCNC particles did not significantly affect the crystallization process of HPP. The crystallization study can further confirm that the percolation threshold of the SDCNC particles in HPP is between 30 and 40 wt.%.

The melting peak temperatures (T_m) of all the SDCNC/HPP composites (Table 4 and Figure 9a), were observed at around 162°C, corresponding to the α-phase crystallite of HPP.[53,54] A notable shoulder at approximately 155°C was observed during the second melting process for composites with the SDCNC loading level at 30 wt.% or above (Figure 9a). The lower melting temperature was identified as the β-phase HPP crystallite,[53] which indicated that the SDCNC particles in HPP matrix promoted the formation of β-phase crystallite of HPP. The appearance of the β-phase crystallite can partially explain the improved impact strength of composites since it has better impact resistance than the α-phase HPP.[53,55,56] The melting enthalpy and crystallinity of the HPP were also plotted against the SDCNC loading levels, and a linear relationship was observed (Figure 9b,c). The crystallinity (X_c) of the HPP increased from 41.3 ± 0.9% to 45.1 ± 0.9% with the incorporation of 50 wt.% SDCNC within the HPP matrix (Table 4). Similarly, the crystallization enthalpies were also observed to be linearly decreasing with the increasing SDCNC loadings (Figure 9b).

3.4 | The effect of MAPP on the properties of SDCNC/HPP composites

The effect of MAPP on the composite behaviors was studied by adding MAPP in 30CNC and 40CNC composites to evaluate the impact at loading levels below and above the percolation threshold. Two-way ANOVA analysis indicated that there is a significant interactive effect between the SDCNC and MAPP content on all mechanical properties, except for tensile MOE and strain properties. Tensile strength and strain increased significantly when introducing MAPP as a compatibilizer in the composites. For example, 30CNC3MAPP and 40CNC3MAPP exhibited a 36% and 61% increase in tensile strain and a 43% and 58% improvement in tensile strength compared with the corresponding SDCNC/HPP composites (Table 5). The increment was ascribed to the enhanced compatibility between the SDCNC particles and HPP matrix, as shown in Figure 2g,h. Compared with the 30CNC composite (Figure 2d), no separated interfaces or gaps between SDCNC particles and matrix were observed, and all SDCNC particles were covered by polymer (Figure 2g,h), increasing the whole composite's continuity and promoting the effective stress transfer from matrix to SDCNC particles. These results indicated that MAPP served as an excellent compatibilizer for SDCNC/HPP composite by establishing improved interfacial adhesion. Statistically, there are no significant differences in the tensile strength and strain under the same SDCNC loading with various MAPP levels (Table 5). In the case of tensile MOE, the SDCNC particle loading level had a substantial effect, whereas the MAPP content had no significant impact (Table 5). This can be explained by the fact that MOE is unaffected by the particle/matrix interfacial adhesion quality in particle-polymer composite systems.[21]

Flexural strength was reported as the stress at 5% strain for all SDCNC/MAPP/HPP composites (no yield or break before 5% strain according to the ASTM D790-A). A similar trend was observed regarding the flexural strength of the composites with MAPP (Table 5). Flexural strength was significantly improved up to 53.0 ± 0.9 MPa (30CNC7MAPP) and 57.3 ± 0.4 MPa (40CNC3MAPP), representing 25% and 45% higher than the corresponding values of 30CNC and 40CNC. Flexural MOE significantly decreased after adding MAPP (Table 5). Generally,

TABLE 5 The mechanical properties of all SDCNC/MAPP/HPP composites.

	Tensile properties			Flexural properties		
Composites	MOE (GPa)	Strength (MPa)	Strain (%)	MOE (GPa)	Strength[a] (MPa)	Impact strength (kJ m^{-2})
30CNC	2.38 ± 0.10[b] B[c]	22.6 ± 0.3 C	3.9 ± 0.3 C	2.04 ± 0.02 D	42.4 ± 0.3 D	1.95 ± 0.21 B
30CNC3MAPP	2.20 ± 0.05 B	32.4 ± 0.1 A	5.3 ± 0.1 A	1.87 ± 0.02 E	51.8 ± 0.6 C	2.72 ± 0.10 A
30CNC5MAPP	2.28 ± 0.07 B	32.5 ± 0.2 A	5.2 ± 0.4 A	1.91 ± 0.03 E	52.8 ± 0.7 C	2.81 ± 0.09 A
30CNC7MAPP	2.30 ± 0.04 B	32.4 ± 0.5 A	5.1 ± 0.4 AB	1.91 ± 0.03 E	53.0 ± 0.9 C	2.73 ± 0.09 A
40CNC	2.68 ± 0.12 A	20.3 ± 0.4 D	2.8 ± 0.1 D	2.46 ± 0.02 A	39.5 ± 0.5 E	1.48 ± 0.25 C
40CNC3MAPP	2.68 ± 0.06 A	32.1 ± 0.2 AB	4.5 ± 0.3 BC	2.25 ± 0.03 B	57.3 ± 0.4 A	2.68 ± 0.10 A
40CNC5MAPP	2.69 ± 0.06 A	31.4 ± 0.4 B	4.8 ± 0.4 AB	2.19 ± 0.04 C	55.9 ± 0.9 B	2.82 ± 0.14 A
40CNC7MAPP	2.69 ± 0.04 A	32.0 ± 0.4 AB	4.6 ± 0.4 AB	2.21 ± 0.03 BC	56.4 ± 0.5 AB	2.72 ± 0.16 A

[a]Flexural strength was reported at yield point for 30CNC and 40CNC and at 5% strain limit for others.
[b]Mean value and standard deviation.
[c]For each column, different letters represent the significant difference ($p < 0.05$). Two-way ANOVA followed with Tukey post-hoc process was used to statistically analyze all data.

polymer with a higher melt flow index indicates a lower molecular weight, which has a lower stiffness.[48,57] Based on the rule of mixtures, adding MAPP with the higher melt flow index (115 g 10 min^{-1}) compared with HPP (20 g 10 min^{-1}), SDCNC/MAPP/HPP composites have lower flexural MOE values.

The addition of MAPP significantly increased the impact strength (Table 5). The impact strengths of 30CNC5MAPP and 40CNC5MAPP are 2.81 ± 0.09 and 2.82 ± 0.14 kJ m^{-2}, representing a 44% and 91% improvement over 30CNC and 40CNC and a 59% enhancement over neat HPP (1.77 ± 0.20 kJ m^{-2}). This dramatic increment is associated with the improved compatibility between the matrix and the SDCNC particles, visible in SEM micrographs (Figure 2g,h). The introduction of MAPP resulted in a new layer of polymer coating on the SDCNC particle surfaces, achieving polymer fracture, and increased toughness. Chemical interactions between SDCNC, MAPP, and HPP occurred. The possible interfacial interaction can be interpreted by the creation of covalent (ester linkages between SDCNC and MAPP) and hydrogen (the interaction between anhydride groups and hydroxyl groups of SDCNC) bonds.[51,58] The similar chemical structure of the PP moiety of MAPP and HPP matrix permits good miscibility and strengthens the interfacial adhesion of the composite. The improved interfacial adhesion, in turn, contributes to mechanical property enhancement. At the same SDCNC loading level, no significant difference in impact strength was observed for the SDCNC/MAPP/HPP composites with varying MAPP contents.

The chemical bonding between SDCNC and MAPP subtly changed the interaction between SDCNC particles and water molecules and decreased the interfacial space in the composites, leading to a change in water gain. When SDCNC particles loading is 30 wt.%, the effect of MAPP on the water absorption behavior was limited because the chemical bonding was occurred between MAPP and individual SDCNC particles or local agglomerates. For SDCNC/MAPP/HPP composite at 40 wt.% SDCNC loadings, the water gain decreased significantly (>14%) with slight variations at 3, 5, and 7 wt.% MAPP loadings (Figure 5b and Table 3). The water diffusion coefficient also decreased notably. The water absorption behaviors of the composite with the SDCNC percolation networks were significantly changed by the reduced interfacial space and the interaction between MAPP and the SDCNC particles. Another possible reason for the decreased water gain is the effective interaction of MAPP and SDCNC, improving SDCNC particle dispersion and distribution and reducing the probabilities of forming multiple SDCNC percolation networks. The decreased water gain to SDCNC loading level ratios (Table 3) confirmed this theory.

Including MAPP in SDCNC/MAPP/HPP composites decreased T_c (Table 4 and Figure 10). Replacing the HPP with 3 wt.% of MAPP decreased the T_c from 124.5 ± 0.2 and 124.4 ± 0.6 for 30CNC and 40CNC to 120.1 ± 0.3 and 120.8 ± 0.7°C, respectively. The addition of MAPP at 5 and 7 wt.% slightly decreased the T_c further (Table 4). MAPP limited the nucleation function of SDCNC on the HPP, possibly obstructing the formation and growth of HPP crystallite on the SDCNC surface. The chemical bonding between MAPP and SDCNC covered the SDCNC particle surface with a different interphase layers, reducing the number of nucleating sites supported by SDCNC

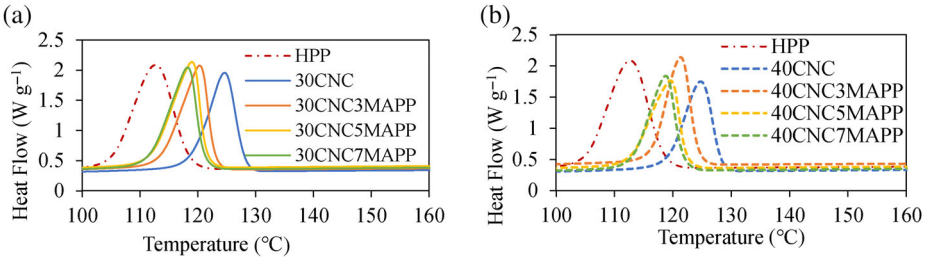

FIGURE 10 The crystallization exothermal curves of SDCNC/MAPP/HPP composites at 30 wt.% (a) and 40 wt.% (b) SDCNC loading level. [Color figure can be viewed at wileyonlinelibrary.com]

and delaying the crystallization process. However, the crystallization peak temperatures of HPP in the SDCNC/MAPP/HPP composites are still higher than that of neat HPP. The change of the SDCNC nucleation function by MAPP may not be able to completely diminish the nucleating effect of SDCNC particles. The other reason is that introducing MAPP may result in a different nucleation mechanisms, changing the crystallization peak temperatures. The effects of the MAPP loading levels on the composite melting behaviors and degrees of crystallinity were also studied, and the results are included in Table 4. No notable changes in melting and crystallinity were observed.

4 | CONCLUSIONS

The study explored the percolation threshold of the SDCNC particles in HPP composites and assessed its influence on the mechanical, morphological, and thermal properties of the SDCNC/HPP composites. Water absorption measurement of the composites helped predict the percolation threshold and the internal structure changes of the composites. Additionally, the effect of MAPP as a compatibilizer (3, 5, and 7 wt.%) on the composite percolation network, mechanical, and thermal properties was investigated.

The mechanical properties of the SDCNC/HPP composites showed that incorporating SDCNC particles improved tensile and flexural MOE significantly by up to 123% and 117% at the highest loading levels compared with the neat HPP. Notably, impact strength was significantly improved by adding 20 and 30 wt.% SDCNC, followed by a subsequent decrease at higher loadings, indicating that percolation networks were formed probably between 30 and 40 wt.% of the SDCNC particles. The results of water absorption measurements confirmed the percolation threshold value of the SDCNC particles in HPP composites, as the water gain changed dramatically above 30 wt.% SDCNC loading, indicating a notable change in the internal structure or distribution of the SDCNC particles in the composites. The hypothesis that water absorption behaviors of the composites can be used to identify the particle percolation threshold is confirmed. Simultaneously, the mechanical properties decreased significantly above the SDCNC percolation threshold. Moreover, SDCNC particles acted as nucleating agents, elevating crystallization peak temperature and crystallinity. Above the SDCNC percolation threshold, the crystallization behavior of HPP in the SDCNC/HPP composites remained relatively unchanged due to the saturated nucleation function provided by the SDCNC particles at the percolation threshold.

The addition of MAPP had a limited influence on the internal structure of the 30CNC composite but a more significant impact on the 40CNC composites based on the moisture absorption measurement. At the 40 wt.% SDCNC loading level, which is above the percolation threshold, the tensile strength, tensile strain, flexural strength, and impact strength of the SDCNC/MAPP/HPP composites were significantly enhanced compared with the corresponding SDCNC/HPP composites, increasing by up to 58%, 61%, 45%, and 91%, respectively. These improvements were ascribed to the effective interfacial adhesion between the SDCNC particles and the matrix promoted by MAPP. Various MAPP contents in the composites provided similar mechanical behaviors. The introduction of MAPP also changed the crystallization process of HPP in the SDCNC/MAPP/HPP composites, restricting the nucleation function of SDCNC and hindering the formation and growth of the crystallites of HPP on the SDCNC surface. Therefore, based on the findings from the research, understanding the percolation threshold of SDCNC particles in HPP matrix can achieve the high potential of SDCNC in polymer composites, and designing the composite with the remarkable performance is achievable, which can be used in automobile, constructure, and furniture and so on.

AUTHOR CONTRIBUTIONS

Xueqi Wang: Conceptualization (supporting); data curation (lead); formal analysis (lead); methodology (equal); validation (lead); visualization (equal); writing – original draft (equal). **Pixiang Wang:** Data curation (supporting); formal analysis (supporting); investigation (supporting). **Shaoyang Liu:** Resources (supporting); validation

(supporting); visualization (supporting); writing – review and editing (supporting). **Ke Zhan:** Formal analysis (supporting). **Brian Via:** Writing – review and editing (supporting). **Tom Gallagher:** Visualization (supporting); writing – review and editing (supporting). **Mathew Smidt:** Writing – review and editing (supporting). **Douglas J. Gardner:** Writing – review and editing (supporting). **Thomas Elder:** Resources (supporting); validation (supporting); writing – review and editing (supporting). **Yucheng Peng:** Conceptualization (lead); methodology (equal); project administration (lead); resources (lead); supervision (lead); visualization (equal); writing – original draft (equal); writing – review and editing (lead).

ACKNOWLEDGMENTS

This work is supported by the Downed Timber Research Program funded by the USDA Forest Service Southern Research Station and the United States Endowment for Forestry and Communities. This research is also supported by the Alabama Agricultural Experiment Station and the Hatch program of the USDA National Institute of Food and Agriculture (ALA031-1-19091). Additional funding support from the USDA National Institute of Food and Agriculture McIntire Stennis project (ALAZ00079) is appreciated.

CONFLICT OF INTEREST STATEMENT

The authors do not have any conflicts of interest.

DATA AVAILABILITY STATEMENT

The authors declare the availability of data and materials on request.

ORCID

Yucheng Peng https://orcid.org/0000-0001-7413-5352

REFERENCES

[1] W. S. Hao, M. Z. Wang, F. S. Zhou, H. Z. Luo, X. Xie, F. L. Luo, R. T. Cha, *Carbohydr. Polym.* **2020**, *243*, 116466.
[2] S. Spoljaric, A. Genovese, R. A. Shanks, *Composites, Part A* **2009**, *40*, 791.
[3] M. K. Singh, A. K. Mohanty, M. Misra, *Composites, Part B* **2023**, *263*, 110852.
[4] A. Chafidz, M. A. H. Ali, R. Elleithy, *J. Mater. Sci.* **2011**, *46*, 6075.
[5] S. Y. Fu, B. Lauke, E. Mäder, C. Y. Yue, X. Hu, *Composites, Part A* **2000**, *31*, 1117.
[6] S. Ghoshal, P. H. Wang, P. Gulgunje, N. Verghese, S. Kumar, *Polymer* **2016**, *100*, 259.
[7] Y. C. Peng, M. Musah, B. Via, X. Q. Wang, *J Compos Sci*, **2021**, *5*, 302.
[8] H. G. B. Premalal, H. Ismail, A. Baharin, *Polym. Test.* **2002**, *21*, 833.
[9] S. Shajari, M. Arjmand, S. P. Pawar, U. Sundararaj, L. J. Sudak, *Composites, Part B* **2019**, *165*, 662.
[10] D. Ndiaye, L. M. Matuana, S. Morlat-Therias, L. Vidal, A. Tidjani, J. L. Gardette, *J. Appl. Polym. Sci.* **2011**, *119*, 3321.
[11] H. Chandekar, V. Chaudhari, S. Waigaonkar, A. Mascarenhas, *Polym. Compos.* **2020**, *41*, 1447.
[12] S.-K. Yeh, C.-C. Hsieh, H.-C. Chang, C. C. Yen, Y.-C. Chang, *Composites, Part A* **2015**, *68*, 313.
[13] B. Kaynak, M. Spoerk, A. Shirole, W. Ziegler, J. Sapkota, *Macromol. Mater. Eng.* **2018**, *303*, 1800037.
[14] M. Liu, S. Tong, Z. Tong, Y. Guan, Y. Sun, *J. Appl. Polym. Sci.* **2023**, *140*, e53671.
[15] P. Song, B. Liu, C. Liang, K. Ruan, H. Qiu, Z. Ma, Y. Guo, J. Gu, *Nano-Micro Lett.* **2021**, *13*, 1.
[16] L. Wang, Z. Ma, H. Qiu, Y. Zhang, Z. Yu, J. Gu, *Nano-Micro Lett.* **2022**, *14*, 224.
[17] H. Sojoudiasli, M. C. Heuzey, P. J. Carreau, *Polym. Compos.* **2018**, *39*, 3605.
[18] Y. C. Peng, D. J. Gardner, Y. Han, *Cellulose* **2015**, *22*, 3199.
[19] X. Q. Wang, P. X. Wang, S. Y. Liu, J. Crouse, D. J. Gardner, B. Via, T. Gallagher, T. Elder, Y. C. Peng, *Polym. Compos.* **2023**, Epub ahead of print.
[20] Y. C. Peng, S. A. Gallegos, D. J. Gardner, Y. Han, Z. Y. Cai, *Polym. Compos.* **2016**, *37*, 782.
[21] S. Y. Fu, X. Q. Feng, B. Lauke, Y. W. Mai, *Composites, Part B* **2008**, *39*, 933.
[22] F. Bettaieb, R. Khiari, A. Dufresne, M. F. Mhenni, M. N. Belgacem, *Carbohydr. Polym.* **2015**, *123*, 99.
[23] H. M. Ng, L. T. Sin, S. T. Bee, T. T. Tee, A. R. Rahmat, *Polym.-Plast. Technol. Mater.* **2017**, *56*, 687.
[24] M. Rinaldi, M. Bragaglia, F. Nanni, *Compos. Struct* **2023**, *305*, 116459.
[25] T. Kuang, M. Zhang, F. Chen, Y. Fei, J. Yang, M. Zhong, B. Wu, T. Liu, *Adv. Compos. Hybrid Mater.* **2023**, *6*, 48.
[26] C. W. Miao, W. Y. Hamad, *Curr. Opin. Solid State Mater. Sci.* **2019**, *23*, 100761.
[27] R. D. Corder, P. Adhikari, M. C. Burroughs, O. J. Rojas, S. A. Khan, *Soft Matter* **2020**, *16*, 8602.
[28] J. M. Jardin, Z. Zhang, G. Hu, K. C. Tam, T. H. Mekonnen, *Int. J. Biol. Macromol.* **2020**, *152*, 428.
[29] H. J. Kim, Y. H. Choi, J. H. Jeong, H. Kim, H. S. Yang, S. Y. Hwang, J. M. Koo, Y. Eom, *Macromol. Res.* **2021**, *29*, 720.
[30] A. Santamaria-Echart, L. Ugarte, C. García-Astrain, A. Arbelaiz, M. A. Corcuera, A. Eceiza, *Carbohydr. Polym.* **2016**, *151*, 1203.
[31] L. Forsgren, A. Venkatesh, F. Rigoulet, K. Sahlin-Sjövold, G. Westman, M. Rigdahl, A. Boldizar, *Composites, Part B*, **2021**, *208*, 108590.
[32] A. Redondo, N. Mortensen, K. Djeghdi, D. Jang, R. D. Ortuso, C. Weder, L. T. Korley, U. Steiner, I. Gunkel, *ACS Appl. Mater. Interfaces* **2022**, *14*, 7270.
[33] Chen, Y.; Gan, L.; Huang, J.; Dufresne, A. In *Nanocellulose*, Walter de Gruyter, Berlin, Germany **2019**.
[34] Y. C. Peng, D. J. Gardner, Y. S. Han, *Cellulose* **2012**, *19*, 91.
[35] Y. C. Peng, Y. S. Han, D. J. Gardner, *Wood Fiber Sci.* **2012**, *44*, 448.
[36] Y. C. Peng, D. J. Gardner, Y. Han, Z. Y. Cai, M. A. Tshabalala, *J Colloid Interf Sci* **2013**, *405*, 85.
[37] Y. Habibi, L. A. Lucia, O. J. Rojas, *Chem. Rev.* **2010**, *110*, 3479.

[38] M. A. S. A. Samir, F. Alloin, J. Y. Sanchez, A. Dufresne, *Polymer* **2004**, *45*, 4149.
[39] N. A. Hanid, M. U. Wahit, Q. P. Guo, S. Mahmoodian, M. Soheilmoghaddam, *Carbohydr. Polym.* **2014**, *99*, 91.
[40] T. X. Huang, I. Kwan, K. D. Li, M. Ek, *Composites, Part A* **2020**, *134*, 105894.
[41] J. Agarwal, S. Mohanty, S. K. Nayak, *J Appl Polym Sci* **2020**, *137*, 49291.
[42] Q. Wu, C. A. Liu, S. Li, Y. Yan, S. T. Yu, L. Huang, *Cellulose* **2023**, *30*, 235.
[43] L. F. Ng, M. Y. Yahya, C. Muthukumar, *Polym. Compos.* **2022**, *43*, 203.
[44] Y. Fan, A. Gomez, S. Ferraro, B. Pinto, A. Muliana, V. L. Saponara, *J. Compos. Mater.* **2019**, *53*, 1097.
[45] C. Aumnate, N. Rudolph, M. Sarmadi, *Polymers* **2019**, *11*, 1456.
[46] A. Dufresne, *Mater. Today* **2013**, *16*, 220.
[47] K. Suzuki, A. Sato, H. Okumura, T. Hashimoto, A. N. Nakagaito, H. Yano, *Cellulose* **2014**, *21*, 507.
[48] L. Wang, A. W. Roach, D. J. Gardner, Y. Han, *Cellulose* **2018**, *25*, 439.
[49] D. G. Gray, *Cellulose* **2008**, *15*, 297.
[50] D. T. Quillin, D. F. Caulfield, J. A. Koutsky, *J. Appl. Polym. Sci.* **1993**, *50*, 1187.
[51] E. Bahar, N. Ucar, A. Onen, Y. J. Wang, M. Oksüz, O. Ayaz, M. Ucar, A. Demir, *J. Appl. Polym. Sci.* **2012**, *125*, 2882.
[52] A. Amash, P. Zugenmaier, *Polymer* **2000**, *41*, 1589.
[53] H. B. Chen, J. Karger-Kocsis, J. S. Wu, J. Varga, *Polymer* **2002**, *43*, 6505.
[54] X. C. Wang, R. F. Song, Y. J. Chen, Y. H. Zhao, K. Y. Zhu, X. Y. Yuan, *Compos Sci Technol* **2018**, *164*, 103.
[55] X. X. Li, H. Y. Wu, Y. Wang, H. W. Bai, L. Liu, T. Huang, *Mater. Sci. Eng.* **2010**, *527*, 531.
[56] K. Shirvanimoghaddam, K. V. Balaji, R. Yadav, O. Zabihi, M. Ahmadi, P. Adetunji, M. Naebe, *Composites, Part B* **2021**, *223*, 109121.
[57] M. S. de Carvalho, J. B. Azevedo, J. D. V. Barbosa, *Polym Test* **2020**, *90*, 106678.
[58] J. M. Felix, P. Gatenholm, *J. Appl. Polym. Sci.* **1991**, *42*, 609.

How to cite this article: X. Wang, P. Wang, S. Liu, K. Zhan, B. Via, T. Gallagher, M. Smidt, D. J. Gardner, T. Elder, Y. Peng, *J. Appl. Polym. Sci.* **2024**, e55627. https://doi.org/10.1002/app.55627